Journal of Applied Polymer Science

Experimental and Simulative Investigation into the Mechanical Behaviors of Polypropylene with Craze Damage in Different Weakening Processes

Zijian Wang, Wenting He, Xiao Hu, Yisheng Zhang
State Key Laboratory of Materials Processing and Die and Mould Technology, School of Material Science and Engineering, Huazhong University of Science and Technology, Wuhan 430074, China
Correspondence to: Y. Zhang (E-mail: zhangys_tc@163.com)

ABSTRACT: This article focused on the experimental and simulative investigation into the mechanical behaviors of polypropylene (PP) at different strain rates. With the aim to describe the crazing yielding of PP, an elastoviscoplastic constitutive model with damage behavior was established and embedded into the finite element codes in the Abaqus platform. The simulation results are in good accordance with the experimental ones. Moreover, the influence of different weakening processes on the material properties was explored. In comparison to the nonweakened specimen, the weakened specimen exhibited nonlinear yielding properties under lower stress. Noteworthily, the integral strength of the weakened specimen proves to be linearly dependent on the cross-section area of the weakening zone. Eventually, the damage model of simplified dashboard was utilized to study the damage law of the dashboard with V-shaped weakening line. Results show the crack initially emerged at the weakening line and then rapidly expanded till the ends of the damage, which satisfied the damage requirements of practical dashboard. © 2014 Wiley Periodicals, Inc. J. Appl. Polym. Sci. **2015**, *132*, 41475.

KEYWORDS: applications; properties and characterization; viscosity and viscoelasticity

Received 5 July 2014; accepted 29 August 2014
DOI: 10.1002/app.41475

INTRODUCTION

Nowadays, increasing attention has been paid to the safety performance of vehicles. As one of the most significant safety factors, the dashboard above the supplementary restraint system (SRS) is urged to meet the safety requirements during a crash of vehicles.[1] Concretely speaking, for the purpose of making the SRS break through the soft seamless dashboard and puff out smoothly without any debris, appropriate weakening process is supposed to be performed on the dashboard.[2] Polypropylene (PP), a kind of common plastic, is commonly used for automotive dashboards, of which the material performance has been widely studied by numerous scholars.[3–7] Owing to PP's viscoplasticity,[8] such conditions as temperature and strain diversify its mechanical properties as well as damage performance, to which should be attached importance in the process of studying the complicated mechanical response of PP.

In terms of the mechanical behavior study of polymers, some literatures have reported the deformation damage in solid polymers[9–12] as well as the mechanical behaviors at high strain rates[13–15] by experimental methods. Conversely, several constitutive models were established to predict the complicated mechanical behaviors of thermoplastic and thermoset materials by computer-aided calculations. For instance, the constitutive model such as elasto-plastic models[16–19] and hyperelastic models[20–23] were implemented into software[24] to describe the strain rate and temperature-dependent behavior of polymers. As for these generic models, precise results may not be easily obtained for a specific material, and a series of customized experiments to determine parameters are always required. This inconvenience can be avoided by implementing the mathematical models which can be written for specific material behavior into user-defined subroutines.[24] However, this solution demands additional programming process and compiling software.

On the whole, most of the existed models are the mathematical expressions of tensile curves, without taking specific physical phenomena into consideration. Taking account of the crazing yielding phenomenon of PP, this work proposed an elastoviscoplastic constitutive model with damage behavior, which can accurately predict the mechanical properties with actual physical significance. In this article, the constitutive model was implemented into the finite element codes of Abaqus to perform numerical simulation. The model parameters were optimized in comparison to experimental results.

By far, few studies have reported the influence of the weakening process on mechanical properties of PP. This article innovatively explored the effects of different weakening processes such as punching holes and milling V-shaped cavity on part performance. Furthermore, corresponding analysis and explanations were given by the proposed constitutive model.

CONSTITUTIVE AND DAMAGE MODEL

As shown in Figure 4, when the stress state of PP reaches a critical state under external loads, it yields with rate dependent viscosity. In the neck region (after the yield point), structural transformation spherulite/fibrilla occurs. This new transformed structure which contains oriented crystalline and amorphous regions will greatly affect the plastic yielding of PP, which is a semicrystalline polymer.[25–27] In the uniaxial tensile test, PP yields in a form of crazing, which comprises quantities of cavities formed by microdistortion. Figure 5 shows stress whitening caused by cavitation and orientation. Stress whitening is a visual sign of cavitation and caused by light scattering either by microvoids or by assemblies of nanovoids.[28,29] Figure 5 also indicates the whole bearing area of the specimen changes little; however, crazing actually reduces the bearing area of the material in a microscopic scale according to the characteristic of crazing yielding. Crazing acts in the similar way the macroscopic necking performs, which is characteristic of reduced yield stress and elasticity modulus with increased strain. Based on the characteristics mentioned above, this article established an elastoviscoplastic constitutive model with damage behavior to describe the comprehensive mechanical behaviors of PP.

The elastoviscoplastic sector of the constitutive model refers to the model proposed by Freudenthal,[30] as shown in eq. (1).

$$\begin{cases} \dot{\varepsilon}_{ij}=\dfrac{1}{2G}\dot{s}_{ij}+\dfrac{1-2v}{E}\dot{\sigma}_{kk}\delta_{ij}+\dfrac{1-\dfrac{\sigma_k}{\sqrt{J_2}}}{2\eta}s_{ij} & \sqrt{J_2}>\sigma_k \\ \dot{\varepsilon}_{ij}=\dfrac{1}{2G}\dot{s}_{ij}+\dfrac{1-2v}{E}\dot{\sigma}_{kk}\delta_{ij} & \sqrt{J_2}<\sigma_k \end{cases} \quad (1)$$

where, G, E, v, η, and σ_k denote the shear modulus, elastic modulus, Poisson's ratio, viscosity coefficient, and the shear yield limit of the material, respectively; $s_{ij}$is the deviatoric stress tensor, J_2 is the second invariant of the deviatoric stress tensor.

The following damage sector which usually characterizes the damage behavior of concrete is applied to depict the damage behavior of the crazing of PP, as eq. (2) shows.

$$\sigma=(1-d)\,\mathbf{D}_0^e(\varepsilon-\varepsilon^{vp}) \quad (2)$$

where $\mathbf{D}_0^e$ is the initial elastic matrix, d evaluates the damage degree, which is a function of inelastic equivalent strain $\bar{\varepsilon}^{vp}$, as shown in eq. (3).

$$d(\bar{\varepsilon}^{vp})=\frac{\bar{\varepsilon}^{vp}-\bar{\varepsilon}_0^{vp}}{\bar{\varepsilon}_f^{vp}-\bar{\varepsilon}_0^{vp}} \quad (3)$$

where $\bar{\varepsilon}_0^{vp}$means the inelastic equivalent strain when the damage begins, $\bar{\varepsilon}_0^{vp}$ is the inelastic equivalent strain when the material is damaged completely, $\bar{\varepsilon}^{vp}$is the current inelastic equivalent strain.

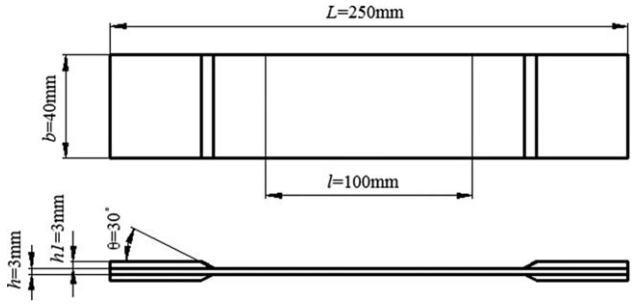

Figure 1. The standard tensile specimen.

With the combination of both sectors above, an elastoviscoplastic constitutive model with damage behavior was proposed in this study, as shown in eq. (4).

$$\begin{cases} \dot{\sigma}_{ij}=2G\left(\dot{\varepsilon}_{ij}-\dfrac{1-\sigma_k/\sqrt{J_2}}{2\eta}s_{ij}\right)+\dfrac{E\dot{\varepsilon}_{kk}}{3(1-2v)}\delta_{ij} \\ \sigma^{m+1}=(1-d)\left(\sigma^m+\Delta t\dot{\sigma}_{ij}\right) \qquad \sqrt{J_2}>\sigma_k \\ \dot{\sigma}_{ij}=2G\dot{\varepsilon}_{ij}+\dfrac{E\dot{\varepsilon}_{kk}}{3(1-2v)}\delta_{ij} \\ \sigma^{m+1}=(1-d)\left(\sigma^m+\Delta t\dot{\sigma}_{ij}\right) \qquad \sqrt{J_2}<\sigma_k \end{cases} \quad (4)$$

where m means the incremental step and Δt is the time increment.

EXPERIMENTAL

Materials and Tensile Tests

The PP homopolymer Grade T30S with its density of 0.9 g/cm^3 (manufacturer data) and melt flow index of 4 g/10 min (for 230°C, 2.16 kg according to ISO 1133) used in this work were supplied by Wuhan Petrochemical (China). The samples for mechanical studies were prepared in the following way: samples were cutoff from a thick film with 3 mm in thickness, obtained by compression moulding at temperature of 230°C and cooled between metal plates. The samples were shaped according to ISO 527 standard. AG-IC 100KN tensile testing machine was applied to test the tensile properties of PP. Figure 1 shows the geometrical dimensions of the specimen.

The deformation dl-load F-curve can be obtained from the tensile tests. According to the deformation dl and load F, corresponding stress–strain curves can be calculated by eqs. (5) and (6).

$$\varepsilon=\ln\left(\frac{dl}{l}+1\right) \quad (5)$$

$$\sigma=\frac{F}{A}=\frac{F}{bh} \quad (6)$$

The Damage Experiment of Simplified Dashboard Model

The actual automobile dashboard is of big size and very expensive, so it is necessary to use a simplified model to study the damage law of the dashboard. To be concrete, only the upper part of the dashboard was considered as the research object and the curved surface was simplified as plane. With the aim to accurately investigate the cracking law of the dashboard, the

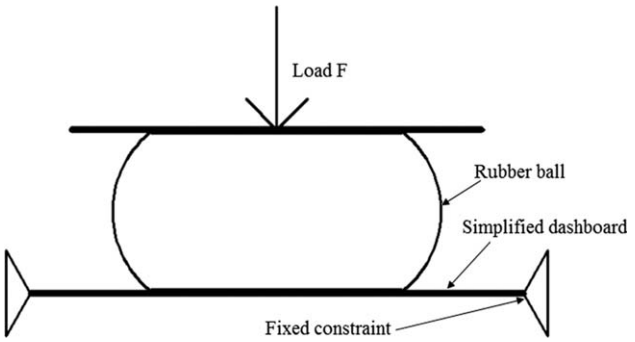

Figure 2. Schematic diagram of the damage test of the simplified dashboard model.

combination of experimental and simulative methods was applied to explore it. Figure 2 shows the schematic diagram of the damage test of the simplified dashboard model.

In this test, under the pressure of the tensile testing machine, a rubber ball filled with gas was used to break the simplified model of the automobile dashboard, to simulate the interaction between SRS and the dashboard. Then the stroke-load curve was read from the testing machine and the cracking load was obtained. The practical tests and main equipment are shown in Figure 3.

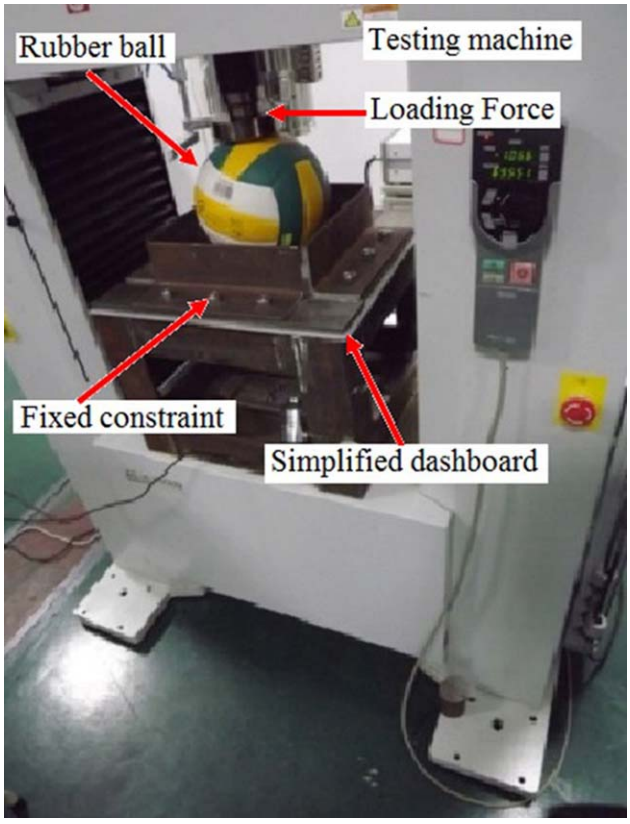

Figure 3. The physical map of the damage test of the simplified dashboard model. [Color figure can be viewed in the online issue, which is available at wileyonlinelibrary.com.]

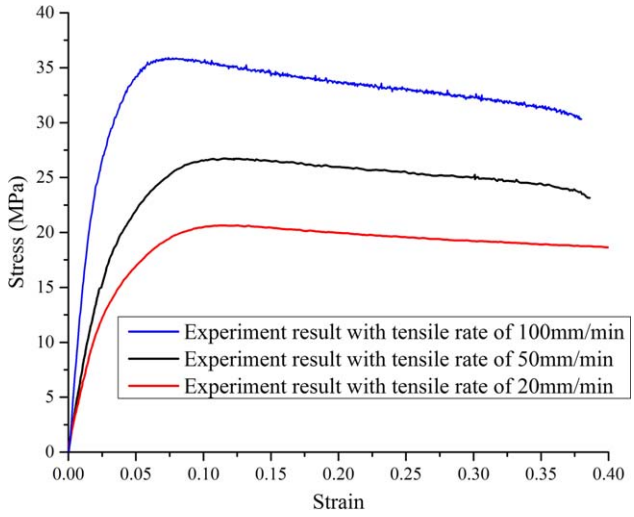

Figure 4. Stress–strain curves of standard specimens at different tensile rates. [Color figure can be viewed in the online issue, which is available at wileyonlinelibrary.com.]

Simulative Methods

In this article, the elastoviscoplastic constitutive model with damage behavior was written into the user subroutine in Abaqus by PC-FORTRAN language. Meanwhile, the parameters required in the constitutive model were optimized by the experimental results, thus making the simulation results more accurate and reliable. To be more specific, the actual stress–strain curves at different tensile rates were obtained during the tensile tests, which will be compared with the corresponding simulation results to optimize the simulation parameters. Finally, the optimal group of parameters was utilized in the damage simulation of the simplified dashboard model. The simulation results can facilitate the design of the process parameters and predict the experimental results of the damage test, thus reducing the cost of trial and error methods.

RESULTS AND DISCUSSION

Tensile Test Results of Standard Specimens

Figure 4 shows the stress–strain curves of the standard specimens at different tensile rates. All of the stress–strain curves at different tensile rates softened, that is to say, the yield stress declined with the increased strain. In addition, with the increase

Figure 5. Stress whitening resulted from the cavitation and orientation. [Color figure can be viewed in the online issue, which is available at wileyonlinelibrary.com.]

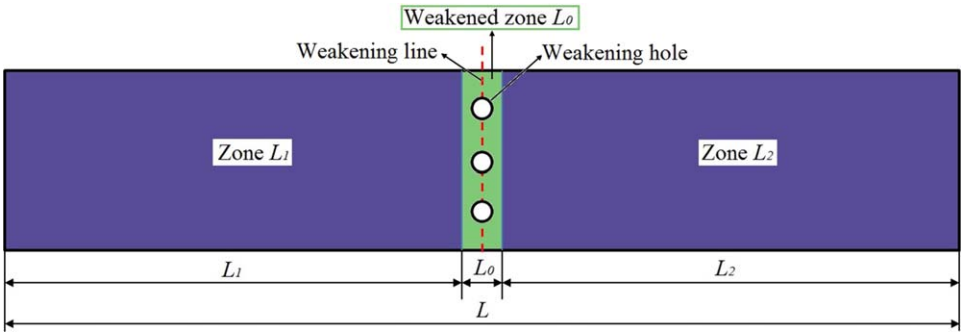

Figure 6. The schematic diagram of the weakened specimen. [Color figure can be viewed in the online issue, which is available at wileyonlinelibrary.com.]

of the tensile rate, the yield stress increased, and the material exhibited viscoplasticity. Figure 5 displays the stress whitening resulted from the cavitation and orientation.

Tensile Test Results of Weakened Specimens

In this section, three holes with 3 mm in diameter were punched in the direction of width in the center of the specimen to weaken it, as shown in Figure 6. Corresponding tensile test results of the weakened specimens are drawn in Figure 7. It can be estimated that weakening the specimen with punching holes has little effect on part strength, however, plays an important role in affecting the plastic strain during the damage. As a result, the plastic strains of the standard and weakened specimens are 0.41 and 0.06, respectively. Meanwhile, the weakening holes reduce the elastic modulus of the specimen.

However, the stress–strain curves in Figure 7 can not reflect the true mechanical properties of the weakened zone L_0. During the whole tensile process, zone L_1 and L_2 only deformed elastically. However, L_0 is the affected area by weakening holes, which deformed elastically in the initial stage of the tensile process and then deformed plastically due to the weakening holes till the specimen's failure. In this study, the measured total strain ε in the tensile test is displayed in eq. (7) and the strain $\varepsilon_0$of the weakened affected area is calculated as eq. (8), where dl_0, dl_1, and dl_2 are assumed as the deformation of zone L_0, L_1, and L_2.

$$\varepsilon=\ln\left(\frac{dl_0+dl_1+dl_2}{l_0+l_1+l_2}+1\right) \tag{7}$$

$$\varepsilon_0=\ln\left(\frac{dl_0}{l_0}+1\right) \tag{8}$$

Due to the pure elastic deformation which occurred in zone $L1$ and $L2$, $dl1$ and $dl2$ can be gained in accordance with the stress–strain curves of the elastic zones of the standard specimen. Besides, dl_0 can be calculated based on the eq. (9), where dl is the total deformation and $\sigma$is its corresponding stress, σ_n (ε) represents the stress–strain curve in the elastic zone of the standard tensile specimen whose inverse function is $\sigma_n^{-1}(\sigma)$. Then ε_0 can be obtained by the combination of eqs. (8) and (9). Finally the calculated stress σ-strain ε_0 curves of the weakened affected area are depicted in Figure 8.

$$dl_0=dl-(l_1+l_2)\times\sigma_n^{-1}(\sigma) \tag{9}$$

Figure 8 reveals that the elastic modulus of the weakened specimen decreased not significantly and due to the concentrated

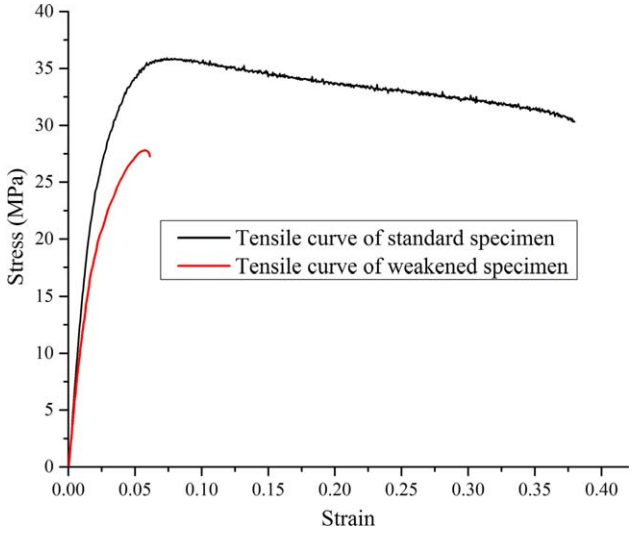

Figure 7. Stress–strain curves of the weakened specimen with punching holes. [Color figure can be viewed in the online issue, which is available at wileyonlinelibrary.com.]

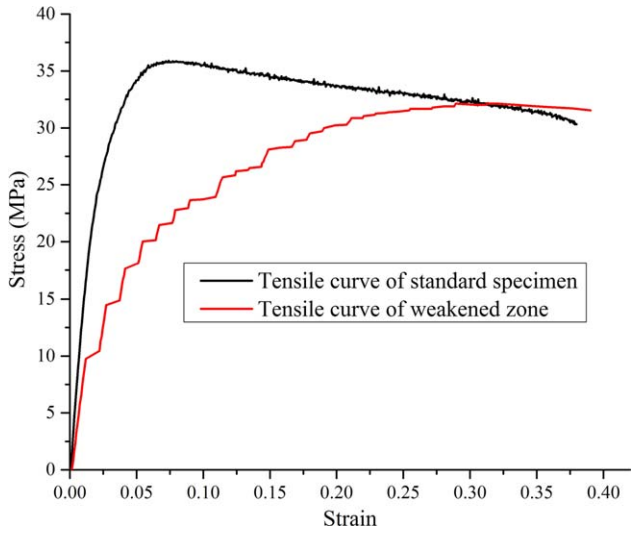

Figure 8. Stress–strain curves of the weakened affected area. [Color figure can be viewed in the online issue, which is available at wileyonlinelibrary.com.]

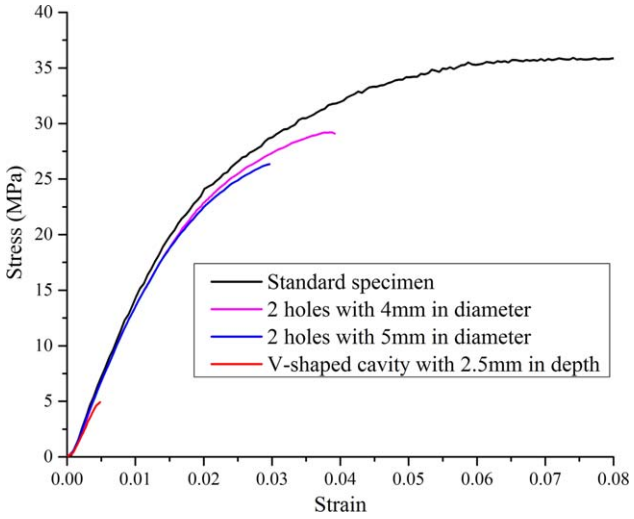

Figure 9. Stress–strain curves of different weakened specimens. [Color figure can be viewed in the online issue, which is available at wileyonlinelibrary.com.]

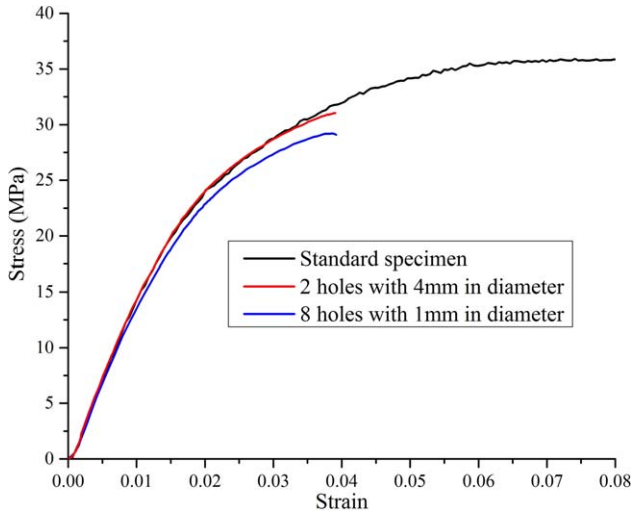

Figure 10. Stress–strain curves of weakened specimens with the same bearing area along the weakening line. [Color figure can be viewed in the online issue, which is available at wileyonlinelibrary.com.]

stress, the weakened specimen yields under lower stress with nonlinear properties. Unlike the strain softening of the standard specimen after yielding, the stress of the weakened increased as the strain rose, which originated from the outward expansion of the plastic area of the weakened zone with the increase of the stress.

The Influence of the Weakening Parameters

To explore the influence of weakening parameters on PP's damage behavior, this paper performed different weakening processes on the standard specimens before the tensile tests. These weakening processes are listed as follows in detail: punching two holes with 4 mm in diameter which are evenly distributed along the weakening line; punching two holes with 5 mm in diameter distributed along the weakening line; and milling a V-shaped cavity with its depth of 2.5 mm and vertex angle of 60° along the weakening line. The integral stress–strain curves of all of these weakened specimens are drawn in Figure 9.

As illustrated in Simulative Methods Section, the integral stress–strain curves in Figure 9 can not exhibit the true mechanical properties of the weakened affected zone. However, the fracture strength shown in this figure can represent the strength of the weakened affected area, as the affected area is the weakest zone throughout the specimen.

It is noted that the strength ratio means the ratio between the strength of weakened specimen and that of the nonweakened; similarly, the bearing area ratio means the ratio between the bearing area along the weakening line of weakened specimen and that of the standard specimen. In our test, the experimental data is reproducible with a strong preference for reproducibility in at least three experiments. The relative error of the tested data in an independent experiment was less than 6%. The standard deviation is given in Table I to evaluate the reproducibility of the experimental data. Table I shows the strength ratio and the bearing area ratio of the weakened specimen are almost the same, with their difference less than 5%, which reveals that the reduced strength of PP in this study was achieved by reducing the bearing area to weaken the material. Therefore, the strength of the weakened zone can be estimated according to the residual bearing area along the weakening line.

Additionally, to further study the impacts of different hole size on part strength with the same bearing area, two more weakening processes were added on the standard specimens, which involve punching two holes with 4 mm in diameter and punching eight holes with 1 mm in diameter. The bearing areas along the weakening line of both weakened specimens are exactly the same, which accounts for four fifths of the original standard specimen. The tensile test curves of both weakened parts are depicted in Figure 10.

Seen from Figure 10, the elongation of both weakened parts stays the same, however, the fracture strength of the weakened parts with the hole diameter of 4 mm turns out to be lower than that with 1 mm in diameter. According to the Westergaard[31] theory of fracture mechanics, the crack stress intensity

Table I. Strength Comparison of Specimens with Differed Weakening Processes

Specimen	Nonweakened	Weakened with two holes with 4 mm in diameter	Weakened with two holes with 5 mm in diameter	V-shaped cavity
Strength (MPa)	35.861 (SD:1.30)	29.169 (SD:1.213)	26.310 (SD:1.137)	4.82 (SD:0.18)
Strength ratio	1	0.8134	0.7337	0.1344
Bearing area ratio	1	0.8	0.75	0.138

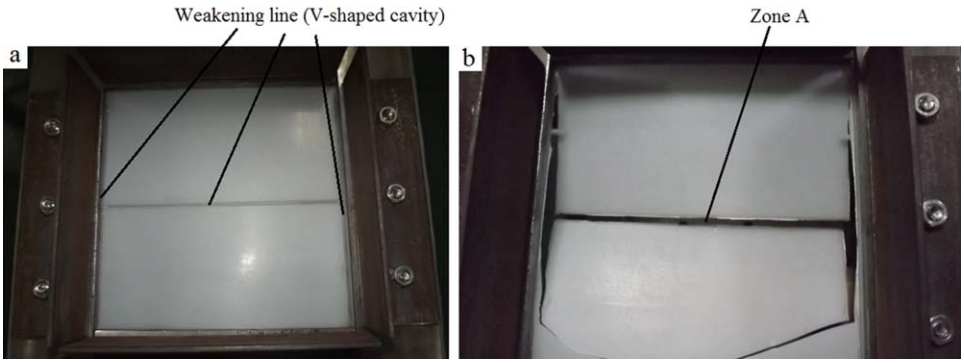

Figure 11. The status of dashboard a) before damage and b) after damage. [Color figure can be viewed in the online issue, which is available at wileyonlinelibrary.com.]

factor KI in elastic region is proportional to the square root of the crack size. That is to say, the induced stress around the holes rises with the increase of hole size. To be specific, the surrounding stress of the weakened holes with 4 mm in diameter is supposed to be twice larger than that with 1 mm in diameter. Therefore, the surrounding area of the weakened holes with 4 mm in diameter stepped into the crazing plastic stage and softened in advance, which further aggravated the weakening of the material during its cracking, thus leading to the lower fracture strength as well as the smaller slope of the tensile curve of the weakened parts with the hole diameter of 4 mm than that with 1 mm in diameter.

Damage Test Results of the Simplified Dashboard Model

Test results in The Influence of the Weakening Parameters Section indicate that punching holes failed to significantly weaken the specimens. Hence, the influence of the weakening of the V-shaped cavity on the damage behavior of PP was investigated by the simplified dashboard model in this section. The V-shaped cavity was milled by tools with its vertex angle of 60° and residual thickness of 0.50 mm. Figure 11 shows the dashboard model before and after damage.

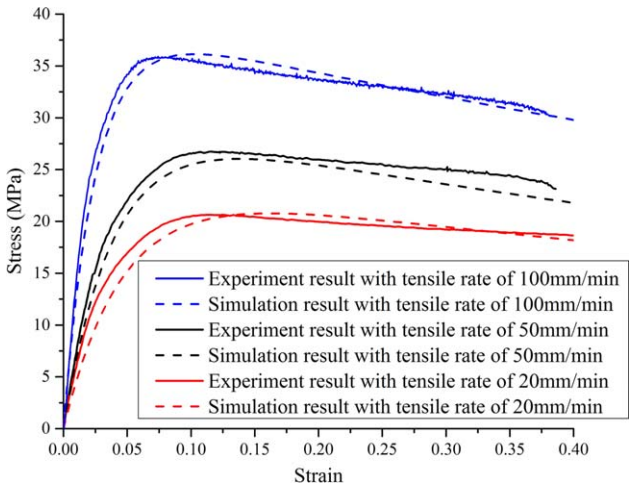

Figure 12. Numerical simulation results of the tensile tests. [Color figure can be viewed in the online issue, which is available at wileyonlinelibrary.com.]

The experimental results above show that due to the significantly reduced fracture strength along the weakening line, the PP specimen initially cracked in zone A in Figure 11, and then split along the weakening line with a part of the matrix material broken. Noteworthily, during the damage test, this piece of matrix material gradually split along the weakening line and did not crack suddenly as a whole, which can be stuck by the foaming and skin layer. It can effectively prevent the whole dashboard from bursting into pieces, which satisfied the demand on the weakening process.

Numerical Simulation Results

Numerical Simulation Results of the Tensile Tests. In this section, the constitutive model proposed in Constitutive and Damage Model Section was implemented into the user subroutine for analysis by Abaqus to obtain the numerical simulation results of the tensile tests. As Figure 12 shows, the simulation results provided by the elastoviscoplastic constitutive model with damage behavior proposed in this study agree well with the experimental results, proving the feasibility and accuracy of this model.

Numerical Simulation of the Weakened Specimen with Punching Holes and the Analytical Solution from Fracture Mechanics. In this section, it is assumed that there exist two holes (cracks) in an infinite plane, which is under the uniaxial stress along *Y*-axis shown in Figure 13. The stress distribution results along *X*-axis obtained by numerical method and analytical method, respectively are drawn in Figure 14, which indicates little difference between both results. Due to the limited mesh size and plane size, the precision of numerical simulation turns out to be lower than that of analytical results. However, the numerical results can still reflect the influence of cracks (namely the holes in this section) on

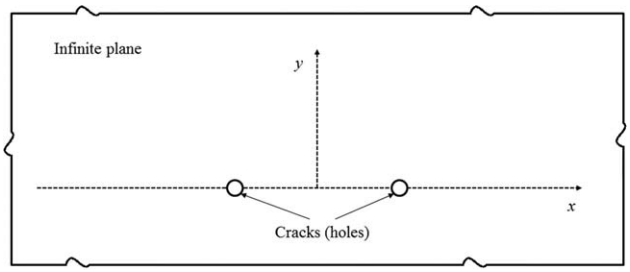

Figure 13. Two micro holes (cracks) in the plane.

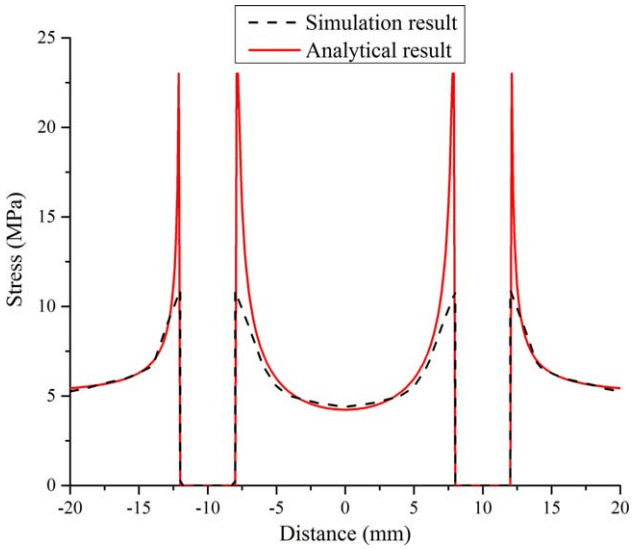

Figure 14. Comparison between analytical and numerical simulation solution. [Color figure can be viewed in the online issue, which is available at wileyonlinelibrary.com.]

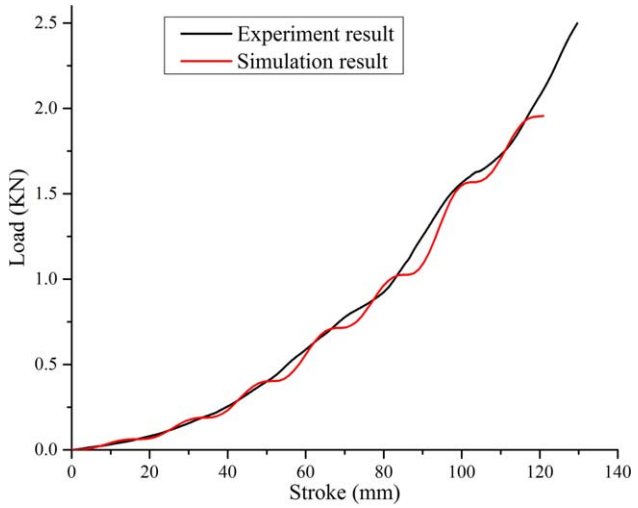

Figure 16. Stroke-load curves of the damage test of the simplified dashboard model obtained by experimental and simulative methods. [Color figure can be viewed in the online issue, which is available at wileyonlinelibrary.com.]

stress distribution. Besides, as the analytical solution in the vicinity of the holes (the crack tips) is singular, the numerical solution differs with the analytical one near the holes.

The comparison between the analytical solution of fracture mechanics and numerical simulation results further validates the effectiveness and reliability of the elastoviscoplastic constitutive model. Moreover, so far, only by idealizing the geometrical morphology of cracks and on the basis of continuum mechanics analysis can the typical quantitative fracture theory be applied successfully to solve the damage problems in the area of fracture mechanics. That is to say, the typical analysis method of fracture mechanics is only appropriate for calculating the mechanical response in the elastic region of parts with simple geometry. Obviously, numerical simulation stands out with huge advantages over the analytical methods.

Numerical Simulation Results of the Damage Test of Simplified Dashboard Model. Seen from the simulated cracking process in Figure 15, the simplified dashboard first cracked at the weakening line and then the cracks rapidly expanded till the end of the damage, which is consistent with the experimental phenomena. Once the state of the meshes at the weakening line reaches the failure condition, the meshes will be deleted. The deleted meshes resulted in the sharp load rise of their

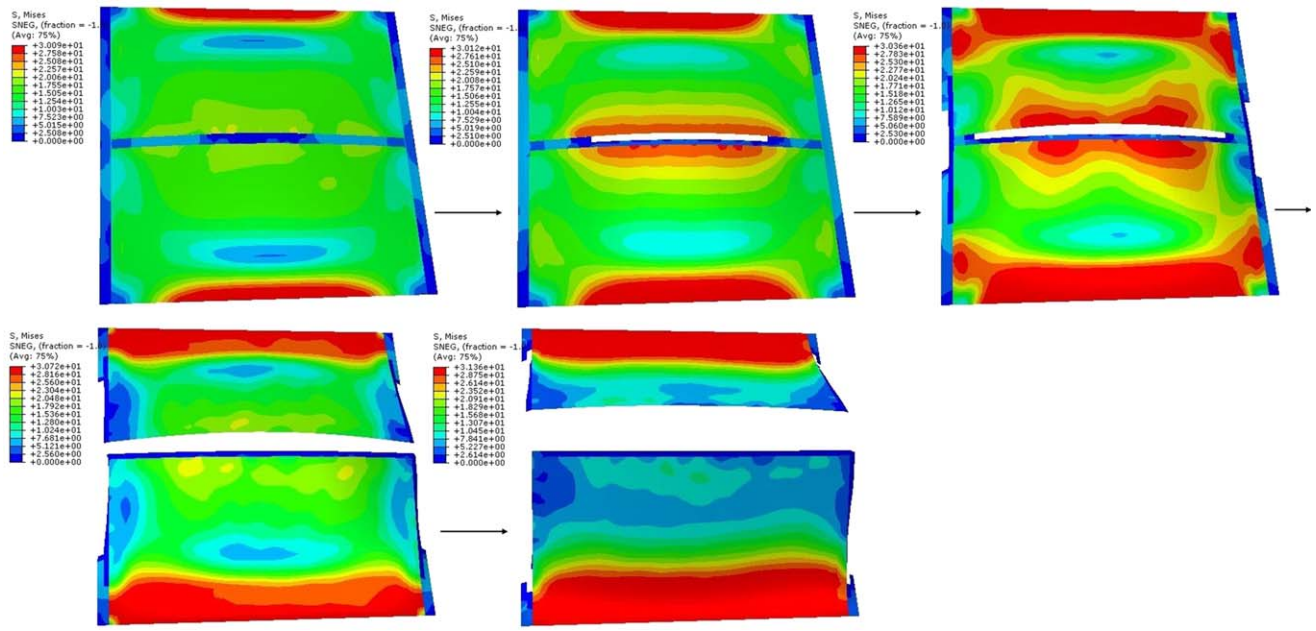

Figure 15. Numerical simulation results of the simplified dashboard model. [Color figure can be viewed in the online issue, which is available at wileyonlinelibrary.com.]

surrounding meshes till the end of the damage, which is equivalent to the rapid expansion of the cracks till the complete failure.

The stroke-load curves obtained by experimental methods and numerical simulation are compared in Figure 16, both of which show a high degree of consistency. Nevertheless, the simulative fracture load turns out to be 2.0KN, lower than that of 2.5KN obtained by experimental measurement. It is because in actual conditions the material properties along the V-shaped cavity differ with that in the direction perpendicular to V-shaped cavity, namely the anisotropy. However, the isotropic material was assumed in the simulation.

CONCLUSIONS

This article focused on the experimental and simulative investigation into the mechanical behaviors of PP with craze damage in different weakening processes. To describe the crazing yielding of PP, an elastoviscoplastic constitutive model with damage behavior was established and embedded into the finite element codes in the Abaqus platform. The influence of different weakening processes on material properties was explored. Unlike the strain softening of the standard specimen after yielding, the stress of the weakened increased as the strain rose. The strength of the weakened zone can be estimated according to the residual bearing area along the weakening line. The simplified model was used to study the damage law of the dashboard, the experimental and simulation results show a high degree of consistency. The crack initially emerged at the weakening line and then rapidly expanded till the end of the damage, which satisfied the damage requirements of practical dashboard. What is more, the comparison between the analytical solution of fracture mechanics and numerical simulation results further validates the effectiveness and reliability of the elastoviscoplastic constitutive model.

ACKNOWLEDGMENTS

This research work is financially supported by the Graduate Innovation and Entrepreneurship Fund of Huazhong University of Science and Technology (HUST, No. 0109070112), the National Natural Science Foundation of China (Grant No. 51275185), and the Fundamental Research Funds for the Central Universities (HUST, No. 0118110621).

REFERENCES

1. Florence, R.; Sherman, K. Trends Driving Design and Materials Changes in the Instrument Panel System, SAE Technical Paper 970445, **1997**, doi: 10.4271/970445.
2. Shin, S. H.; Cheong, C. *Appl. Acoust.* **2010**, *7*, 1162.
3. Şerban, D. A.; Weber, G.; Marşavina, L.; Silberschmidt, V. V.; Hufenbach, W. *Polym. Test.* **2013**, *32*, 413.
4. Huang, J.; Rodrigue, D. *Mater. Des.* **2014**, *55*, 653.
5. Río, T. G.; Salazar, A.; Rodríguez, J. *Mater. Des.* **2012**, *42*, 301.
6. Reis, J. M. L.; Pacheco, L. J.; da Costa Mattos, H. S. *Polym. Test.* **2013**, *32*, 338.
7. Nunes, L. C. S.; Reis, J. M. L.; da Costa Mattos, H. S. *Eng. Fract. Mech.* **2011**, *78*, 2957.
8. Balieua, R.; Lauroa, F.; Bennania, B.; Delillea, R.; Matsumotod, T.; Mottolad, E. *Int. J. Plast.* **2013**, *51*, 241.
9. Tang, C. Y.; Tsui, C. P.; Shen, W.; Li, C. C.; Peng, L. H. *Polym. Test.* **2001**, *20*, 15.
10. Zaïria, F.; Naït-Abdelaziza, M.; Gloaguenb, J. M.; Lefebvreb, J. M. *Int. J. Plast.* **2008**, *24*, 945.
11. Sell, C. G.; Hiver, J. M.; Dahoun, A. *Int. J. Solids Struct.* **2002**, *39*, 3857.
12. Brown, E. N.; Rae, P. J.; Orler, E. B. *Polymer* **2006**, *47*, 7506.
13. Naik, N. K.; Perla, Y. *Polym. Test.* **2008**, *27*, 504.
14. Schoßg, M.; Bieröel, C.; Grellmann, W.; Mecklenburg, T. *Polym. Test.* **2008**, *27*, 893.
15. Mulliken, A. D.; Boyce, M. C. *Int. J. Solids Struct.* **2006**, *43*, 1331.
16. Nunes, L. C. S.; Dias, F. W. R.; da Costa Matos, H. S. *Polym. Test.* **2011**, *30*, 791.
17. Şerban, D. A.; Marşavina, L.; Silberschmidt, V. *Comput. Mater. Sci.* **2012**, *52*, 139.
18. Dunne, F.; Petrinic, N. Introduction to Computational Plasticity; Oxford University Press, **2006**.
19. Rees, D. W. A. Basic Engineering Plasticity; Elsevier: Amsterdam, Netherlands, **2006**.
20. Killian, H. G.; Enderle, H. F.; Unseld, K. *Colloid. Polym. Sci.* **1986**, *264*, 866.
21. Marlow, R. S. In Constitutive Models for Rubber III, Balkema Publishers: London, UK, **2003**.
22. Ogden, R. W. *Proc. R. Soc. Lond. A.* **1972**, *326*, 565.
23. Rivlin, R. S.; Saunders, D. W. *Philos. Trans. R Soc. Lond. A.* **1951**, *251*.
24. ABAQUS Inc. ABAQUS Analysis User's Manual. ABAQUS Inc.: USA, **2008**.
25. Rozanski, A.; Galeski, A. *Int. J. Plast.* **2013**, *41*, 14.
26. Hong, K.; Rastogi, A.; Strobl, G. *Macromolecules* **2004**, *37*, 10165.
27. Lin, J.; Shenogin, S.; Nazarenko, S. *Polymer* **2002**, *43*, 4733.
28. Pawlak, A.; Galeski, A.; Rozanski, A. *Prog. Polym. Sci.* **2014**, *39*, 921.
29. Bartczak, Z.; Morawiec, J.; Galeski, A. *J. Appl. Polym. Sci.* **2002**, *86*, 1413.
30. Freudenthal, A. M. Statistical approach to brittle fracture. In: Fracture, Vol. 2; Liebowitz, H.; Academic press: New York, **1968**; pp. 591–619.
31. Westergaard, H. M. *J. Appl. Mech.* **1939**, *6*, 49.